International Journal of Remote Sensing

ISSN: (Print) (Online) Journal homepage: https://www.tandfonline.com/loi/tres20

The first evaluation of the FY-3D/MERSI-2 sensor's thermal infrared capabilities for deriving land surface temperature in volcanic regions: a case study of Mount Etna

S. Aveni & M. Blackett

To cite this article: S. Aveni & M. Blackett (2022) The first evaluation of the FY-3D/MERSI-2 sensor's thermal infrared capabilities for deriving land surface temperature in volcanic regions: a case study of Mount Etna, International Journal of Remote Sensing, 43:8, 2777-2792, DOI: 10.1080/01431161.2022.2068360

To link to this article: https://doi.org/10.1080/01431161.2022.2068360

Published online: 13 May 2022.

INTERNATIONAL JOURNAL OF REMOTE SENSING
2022, VOL. 43, NO. 8, 2777–2792
https://doi.org/10.1080/01431161.2022.2068360

Taylor & Francis
Taylor & Francis Group

The first evaluation of the FY-3D/MERSI-2 sensor's thermal infrared capabilities for deriving land surface temperature in volcanic regions: a case study of Mount Etna

S. Aveni and M. Blackett

Centre for Agroecology, Water and Resilience, Coventry University, Coventry, UK

ABSTRACT

In November 2017, the China Meteorological Administration launched a new polar orbiting satellite in its Fengyun (FY) series: FY-3D. With its main purpose being the collection of meteorological data, FY-3D featured a comprehensive payload that is equally exploitable by various Earth Science disciplines. One of its sensors, the MEdium Resolution Spectral Imager-2 (MERSI-2), provides visible and infrared imagery at spatial resolutions of 250 – 1000 m. These characteristics make MERSI-2 suitable for volcanological remote sensing and make it comparable to the National Aeronautics and Space Administration's (NASA's) Moderate Resolution Imaging Spectroradiometer (MODIS) sensors which themselves, have been widely used in volcanological applications. This paper evaluates the first clear and near-coincident MODIS – MERSI-2 images of Mount Etna (Italy) during an active volcanic phase in 2019 and in turn, provides the first assessment of MERSI-2's utility in observing volcanic activity in the Thermal InfraRed (TIR). To ensure the comparability of both scenes, data from each were converted to Land Surface Temperature (LST) and comparisons were encouraging, with an r^2 of 0.92, a mean temperature discrepancy of 0.26 K and a root mean squared error of 0.75 K. Having ascertained comparability, we focussed on the absolute temperatures detected at the eruption site, with the highest being 317.3 K and 328.1 K for MODIS and MERSI-2, respectively. The 20 minute gap between the acquisitions is the most likely the cause of this temperature discrepancy, suggesting variations in lava effusion rates and activity were occurring at Mount Etna over such timescales. This study confirms the applicability of MERSI-2 for observing volcanic activity and emphasises the significance of TIR volcanic monitoring and the importance that additional spaceborne platforms might have in reducing temporal gaps between image acquisitions. Given its unique characteristics, future studies should investigate the applicability of MERSI-2 in more varied volcanic settings.

ARTICLE HISTORY
Received 6 January 2022
Accepted 18 April 2022

KEYWORDS
Thermal Infrared; Volcanoes; MODIS; FY-3D; Etna

CONTACT S. Aveni avenis@uni.coventry.ac.uk Centre for Agroecology, Water and Resilience, Coventry University, Coventry, CV1 5FB, UK

1. Introduction

Since the late 1980s, the China Meteorological Administration (CMA) has launched a range of meteorological satellites named Fengyun, or 'wind-cloud' (Lu et al. 2020). The first and third series of these satellites, Fengyun-1 and -3, were polar orbiting and the second and fourth (Fengyun-2 and -4) were geostationary. The Fengyun-3 series was first presented to the world in 2002 (Meng, Sun and Dong 2002) and the first experimental satellite of the range, FY-3A, was launched in 2008, followed by FY-3B and FY-3C in 2010 and 2013, respectively. The missions of the FY-3 series included obtaining three-dimensional thermal and moisture soundings of the atmosphere for input into numerical weather prediction tools and imaging large-scale meteorological/hydrological events for disaster management purposes (Dong et al. 2009). The latest satellite in the FY-3 series, FY-3D, was launched in November 2017. The FY-3D possesses the most comprehensive payload of the FY-3 series, including the MEdium Resolution Spectral Imager-2 (MERSI-2) which is an advanced spectral imager with infrared-observational capabilities and which replaced and merged MERSI on FY-3A/3B and VIRR on FY-3A/3B/3C (i.e. Yang et al. 2019a, 2019b; Wang et al. 2020). With regard to infrared observations, there are a whole host of applications outside of meteorology, including the retrieval of land surface temperatures (LST) which, in the field of geology, has particular utility in the monitoring of volcanic activity (Blackett 2017).

1.1. Remote sensing of volcanic activity

The infrared remote sensing of volcanoes is a discipline that extends back to the early days of Earth observation, with active volcanoes being particularly suited to infrared observation by virtue of their emissions of heat (Oppenheimer 1998). Numerous studies (e.g. Wooster and Rothery 1997; Hirn et al. 2008; Wright, Glaze and Baloga 2011; Vieira, Teodoro and Gomes 2016; Nádudvari et al. 2020) have since demonstrated the direct relationship between infrared emissions and volcanic activity, and have provided crucial information for the volcanological community (for a historical perspective and comprehensive review, see Blackett 2017).

One of the key principles in the remote sensing of volcanic activity is Wien's Displacement Law. This Law shows that the peak wavelength of radiant emissions from an object will decrease as its temperature increases (Wien 1896; Rothery, Francis and Wood 1988). This dictates that at average Earth surface temperatures (e.g. 288 K), the chief wavelengths of radiant emissions will be 7.0 – 15.0 μm (i.e. in the Thermal InfraRed [TIR] portion of the spectrum), whereas those from active volcanic surfaces (which may exceed 1000 K), will be 1.5 – 4.0 μm (i.e. within the ShortWave InfraRed [SWIR] and Middle InfraRed [MIR] portions of the spectrum). Consequently, the SWIR and MIR bands of remote sensors have been regularly used to monitor active volcanism (Francis and Rothery 1987; Rothery, Francis and Wood 1988; Wright, Flynn and Harris 2001; Blackett and Wooster 2011; Marchese et al. 2018; Massimetti et al. 2020) although they have one significant drawback: they are typically associated with a poorer temporal resolution that is sub-optimal for monitoring rapidly changing volcanic activity. The TIR bands of satellite sensors in contrast, possess a higher temporal resolution by virtue of their lower spatial resolution. Fortunately however, the TIR bands do retain sensitivity to the extreme

temperatures associated with volcanism because of the fact that just a small region of intense temperature on the surface will significantly raise the TIR pixel temperatures detected and will thus cause volcanic surfaces to appear anomalous in comparison to their surroundings (e.g. Wright et al. 2002, 2004; Coppola et al. 2015).

To date, the majority of satellite-based volcanological observations have been made using the various National Aeronautics and Space Administration (NASA) series of satellite sensors, for reasons of ease of access, length of timeseries available and indeed, high quality of data provision (Wooster and Rothery 1997; Rothery, Coppola and Saunders 2005; Pieri and Abrams 2005; Murphy et al. 2013; Blackett 2015; Carr, Clarke and Vanderkluysen 2016; Trifonov et al. 2017). Of the NASA satellite series, the MODerate resolution Imaging Spectroradiometer (MODIS) sensor has been most widely applied volcanologically (Wright et al. 2002; Watson et al. 2004; Rothery, Coppola and Saunders 2005; Coppola et al. 2012, 2015). Other agencies, however, have launched comparable satellites, including the European Space Agency with its Copernicus Programme (i.e. Sentinel-2 and Sentinel-3) – the satellites of which have also been used for volcanological observations (Corradino et al. 2019; Massimetti et al. 2020). In contrast, sensors of the CMA are yet to be tried and tested with regard to their volcanological observations and as such, this study will address this omission.

This study will examine MERSI-2 infrared imagery of Mount Etna, taken during an active phase in 2019 and in turn, will provide the first assessment of the sensor's utility in observing thermally anomalous volcanic activity. Confirmation of MERSI-2's volcanological utility, by comparison with concurrent MODIS imagery, will reveal a valid new source of data for the remote study and monitoring of active volcanism.

1.2. The FY-3D satellite and MERSI-2

The payload of FY-3D includes microwave sounders and imagers (MWTS-2, MWHS-2 and MWRI), similar to those on its predecessors, and a new Greenhouse gases Absorption Spectrometer (GAS), Hyperspectral InfraRed Atmospheric Sounder (HiRAS), Global Navigation Satellite System (GNSS) and Occultation Sounder (GNOS) (Wang et al. 2018; Fang 2018; NSMC 2018; EOportal 2021). Of most relevance to this study, however, is MERSI-2, which provides visible and infrared imagery over 25 bands and at spatial resolutions of 250 m – 1000 m (Table 1). The characteristics of MERSI-2 make it comparable to MODIS on-board NASA's Terra and Aqua satellites (Yan et al. 2021). Indeed, Wang et al. (2019a) has shown good agreement in LSTs from MODIS and MERSI-2 but no studies have yet confirmed this agreement with regard to volcanic observations.

2. Methods

2.1. Data acquisition

On 20 July 2019, the first clear and near-coincident MODIS (Aqua) – MERSI-2 image acquisitions occurred. At 00.45 UTC, MODIS acquired TIR imagery of Mount Etna during an active and effusive episode and, 20 min later, FY-3D captured the same event. The MODIS scene was obtained from NASA's Atmosphere Archive & Distribution System (LAADS) Distributed Active Archive Centerin the format of the MODIS Level 1B

Table 1. Medium Resolution Spectral Imager-2 (MERSI-2) bands wavelenght and resolution.

Band	MERSI-2 (μm)	Spatial Resolution (m)	Band	MERSI-2 (μm)	Spatial Resolution (m)
1	0.470	250*	14	0.746	1000
2	0.550	250*	15	0.865	1000
3	0.650	250*	16	0.905	1000
4	0.865	250*	17	0.936	1000
5	1.38	250*	18	0.940	1000
6	1.64	1000	19	1.03	1000
7	2.13	1000	20	3.8	1000
8	0.412	1000	21	4.05	1000
9	0.443	1000	22	7.2	1000
10	0.490	1000	23	8.55	1000
11	0.555	1000	24	10.8	250*
12	0.670	1000	25	12.0	250*
13	0.709	1000			

*The product FY3D_MERSI_GBAL_L1_yymmdd_hhmm_1000M_MS (used in this study) provides these bands as aggregated to 1 km.

Calibrated Radiances product (MYD021 KM) (MCST 2017) in which the radiance data are provided in W/(m^2 μm sr). The corresponding Level 1 FY-3D MERSI-2 product (FY3D_MERSI_GBAL_L1) was downloaded from the Chinese National Satellite Meteorological Centre's Fengyun Satellite Data Center (NSMC 2013), distributed in mW/(m^2 cm^{-1} sr) units.

2.2. Data processing

The following methods were applied in the derivation of LST from the data acquired by each sensor. These methods were equally applicable to the non-volcanic and active volcanic surfaces that were captured on 20 July 2019, with the only difference being the values retrieved, which were, as expected, higher and indeed, more variable between the acquisition times.

In contrast to data from the L1B MODIS product, the MERSI-2 data came as two separate files: one of pixel-level digital numbers (DNs) and one with corresponding georeferencing data. This meant that further data processing was required to access the calibrated radiance data of MERSI-2, and few sources of literature provide much detail on how to do this (CGMS (Coordination Group for Meteorological Satellites) 2018, 2020; Zhang 2019; Zhang et al. 2020). Georeferencing was initially undertaken by deriving a Geographic Lookup Table from the MERSI-2 georeferencing dataset using the ENVI 5.3 software (ENVI-IDL Technology Hall 2014). The 1 km × 1 km pixels of each scene were then aligned to facilitate the objective comparison of the observations of each sensor. Calibration of the MERSI-2 DN values to radiance (L_v, where v is the channel wavenumber in cm^{-1}), in units: mW/(m^2 cm^{-1} sr), was then conducted following Na (2018) and Na et al. (2019) which showed:

$$L_v = DN \times slope + intercept \tag{1}$$

Where: *slope* and *intercept* are available in the metadata.

The comparable TIR bands 32 and 25 from MODIS and MERSI-2, respectively, were those of interest in this study. Despite their similarity in terms of spectral characteristics (Figure 1), their small differences meant that it was not possible to compare their

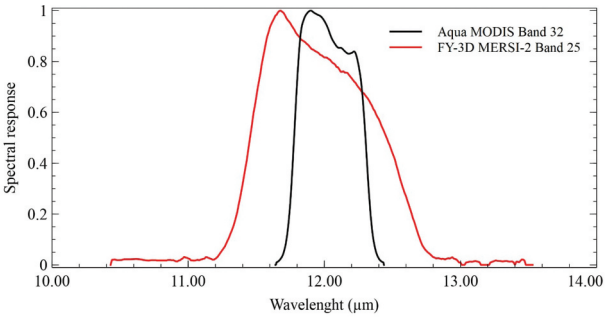

Figure 1. Spectral response functions of FY-3D and MODIS (Aqua) TIR bands 25 (12.00 μm) and 32 (12.02 μm), respectively.

calibrated radiance retrievals directly and as such, these were converted to land surface temperature (LST). The derivation of LST from MODIS calibrated infrared radiance data follows a well-established procedure (e.g. Wan and Snyder 1996; Mao et al. 2005) whereas for MERSI-2 data, some additional steps were required (Wang et al. 2019a). For both datasets, however, the common principle is the fact that the spectral radiance emitted by a black-body at a particular temperature and in a particular wavelength ($L_\lambda(T_S)$), is directly related to its brightness temperature (Ts), according to the Planck Function:

$$L_\lambda(T_s) = \frac{c_1}{\lambda^5\left(e^{\frac{c_2}{\lambda Ts}} - 1\right)} \tag{2}$$

Where: λ is the channel wavelength (in μm), and c_1 and c_2 are constants of 1. 19,104 × 10^8 W/m^2 sr μm^{-4} and 1. 43,877 × 10^4 μm K, respectively (Wang *et al.* 2019b).

By inverting Eq. 2, the temperature of an observed black-body surface can be calculated but, to derive this from the signal detected by a sensor at the top of the atmosphere ($L_\lambda(T_\lambda)$), corrections are needed based on the effects of the atmosphere, in terms of transmittance (τ_λ) and up- and down-welling path radiances ($L_\lambda^{\uparrow}$ and $L_\lambda^{\downarrow}$, respectively) at particular wavelengths (λ), and emissivity and reflectance of the surface (ε_λ and $1 - \varepsilon_\lambda$, respectively). These adjustments can be applied as follows (from Wang et al. 2019a):

$$L_\lambda(T_\lambda) = L_\lambda(T_s)\varepsilon_\lambda\tau_\lambda + L_\lambda^{\uparrow} + (1 - \varepsilon_\lambda)L_\lambda^{\downarrow}\tau_\lambda \tag{3}$$

Following Singh, Satpathy and Jeyaseelan (2010) and Kim et al. (2019), this atmospheric correction was undertaken using the Thermal Atmospheric Correction (TAC) module of the ENVI 5.3 software. This process is again straightforward for MYD021 KM, given that its data are in units W/(m^2 μm sr), however, for FY-3D, prior to this step, the radiance data had to be converted to comparable units from those of its original distribution.

The TAC has long been used to remove atmospheric artefacts from TIR bands acquisitions (i.e. Bustamante et al. 2016, Abdelmalik 2018, Kim et al. 2019), and applies the In-Scene Atmospheric Compensation (ISAC) algorithm developed by Johnson and Young (1998). The method assumes a constant atmosphere layer over a scene and $L_\lambda^{\downarrow} = 0$ (which

is an appropriate assumption in the TIR (DiStasio and Resmini 2010)). It then calculate $L_{\lambda}^{\uparrow}$ and τ_{λ} estimating first the surface temperature of each pixel used to approximate T_S using the Planck function (Eq. 2), assuming $\varepsilon = 1$; and then, fitting a line to a scatter plot of radiance vs. T_S, with $L_{\lambda}^{\uparrow}$ and τ_{λ} derived from the slope and offset of this line, respectively (Anul Haq, Jain and Menon 2012) (for method's details see Young, Johnson and Hackwell 2002). The ENVI module outputs the atmospherically corrected radiance values ($L_{\lambda}(T_{\tau})$) in units W/(m^2 μm sr). Following application of this step, and the methods of Singh, Satpathy and Jeyaseelan (2010) and Dar, Qadir and Shukla (2019), T_S (K) was then derived for the FY-3D data using the inverse Planck function:

$$T_S = \frac{c_2}{\lambda \ln\left(c_1/\lambda^5 L_{\lambda}(T_{\tau})\right) + 1)} \tag{4}$$

And in turn, the *LST* (K) could be derived via inclusion of the emissivity (ε) term and application of the following (from Gupta 2003):

$$LST = \frac{1}{\varepsilon^{\frac{1}{4}}} T_S \tag{5}$$

Values of emissivity were obtained from the MODIS/Aqua Land Surface Temperature/Emissivity Daily L3 Global 1 km SIN Grid (MYD11A1) product but from a slightly earlier date: 6th July, 2019 (the closest, cloud-free image of the surface) (from NASA LP DAAC 2015). Despite the fact that this might slightly differ from the conditions experienced by the investigated scenes at the time of acquisition, its effect on the retrieved LST for the comparative purpose of this study is negligible. In fact, considering the short gap between the acquisitions, it is reasonable to assume that ε remained quasi-identical across the two scenes, allowing an unbiased comparison of the two sensors. Besides, emissivity values ranging from 0.96 to 0.99 used in this work are consistent with those identified by other authors who investigated the LST of Sicily (i.e. Mincapilli et al. 2016), suggesting that ε values used in this work are indeed representative of the investigated region.

With regard to the hot volcanic surface, similar studies conducted on active lava flows at Mount Etna using the TIR portion of the spectrum suggested that a typical and constant ε between 0.95 and 0.98 can be used (Neri et al. 2017; Nádudvari et al. 2020), hence including the emissivity range used in this work.

One additional step was required to extract the LST values from MERSI-2 data: an adjustment based on various band-specific coefficients and as detailed in Na (2018) and Na et al. (2018; 2019). This adjustment had a negligible impact on the outcomes, consisting of multiplying the MERSI-2-derived LST by 1.00065 and the addition of 0.0875 K (where these coefficients were drawn from the Global Attribute metadata of the MERSI-2 file).

3. Results

The calibrated radiance MODIS and MERSI-2 scenes of Sicily from 20 July 2019 are displayed in Figure 2 and their data are compared, at the 1 km pixel level, in Figure 3. The data from each scene agree strongly, with a Spearman's Rank Correlation Coefficient

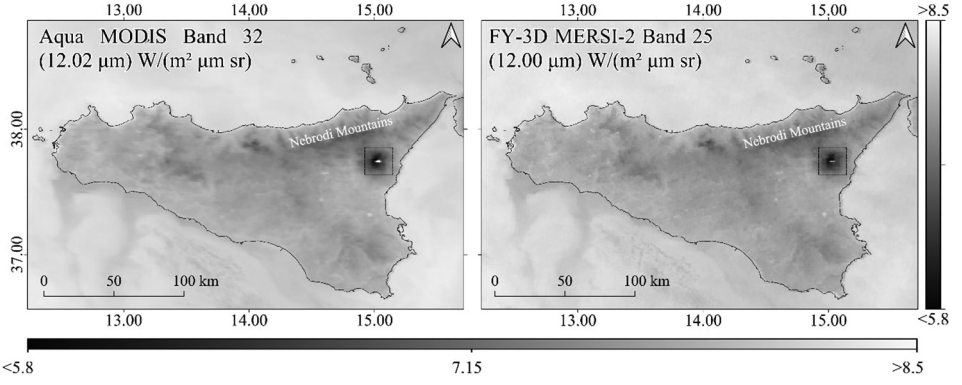

Figure 2. Calibratred radiance scenes of Sicily, as acquired from MODIS and MERSI-2 at 00.45 and 01.05 (UTC), respectively. Both images are displayed in units of W/(m2 µm sr).

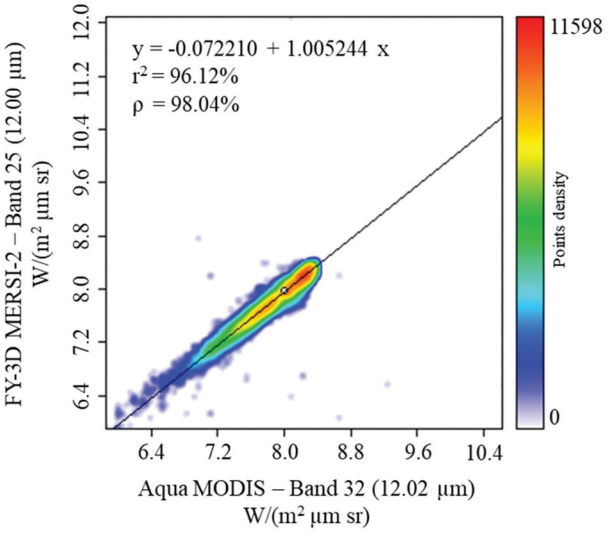

Figure 3. Density plot showing the relationship between MODIS and MERSI-2 radiance values, prior corrections, over 144,139 data points (from Figure 2). Each data point relates to corresponding pixels as imaged by each sensor.

(ρ) = 98.04% and Coefficient of Determination (r^2) = 96.12%. At this wide scale, the small discrepancy in data between both scenes is likely attributable to subtle differences in pixel alignment, image acquisition geometry and time and spectral response.

The corresponding LST data are displayed in Figure 4 and compared in Figure 5. Not unexpectedly, high levels of agreement are again revealed (ρ = 94.48%; r^2 = 91.96 and RMSE = 0.75 K), with very similar whole-scene LST values (290.0 K and 289.8 K for MODIS and MERSI-2, respectively). In fact, the mean temperature discrepancy (ΔT, i.e. the mean LST difference between comparable pixels) for the whole scene of 0.26 K, compares very favourably to that derived from similar comparisons, with Wang et al. (2019a) finding ΔT = 1.37 K in MERSI-2 - MODIS LST comparison. The corresponding statistical distributions of

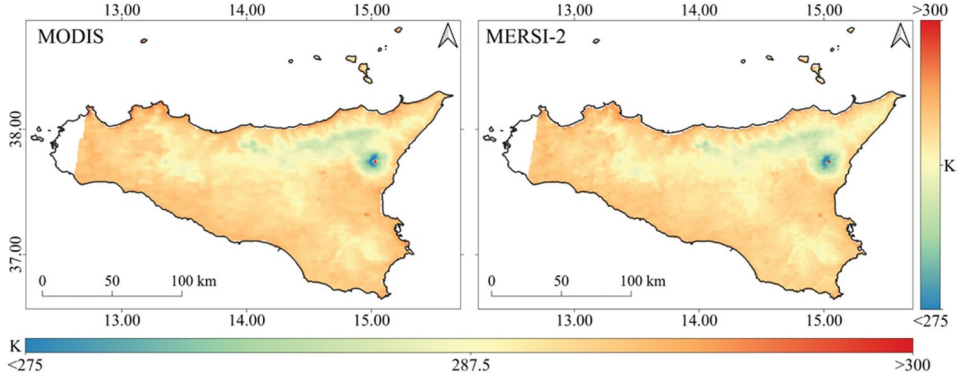

Figure 4. LST (in Kelvin) obtained for the entire Sicily Region from MODIS (Aqua) and MERSI-2, from left to right, respectively. the whole scene mean LSTs are 290.0 K and 289.8 K for MODIS and MERSI-2, respectively. the missing data to the west of Sicily is due to a gap in data from the MODIS emissivity product (MYD11A1).

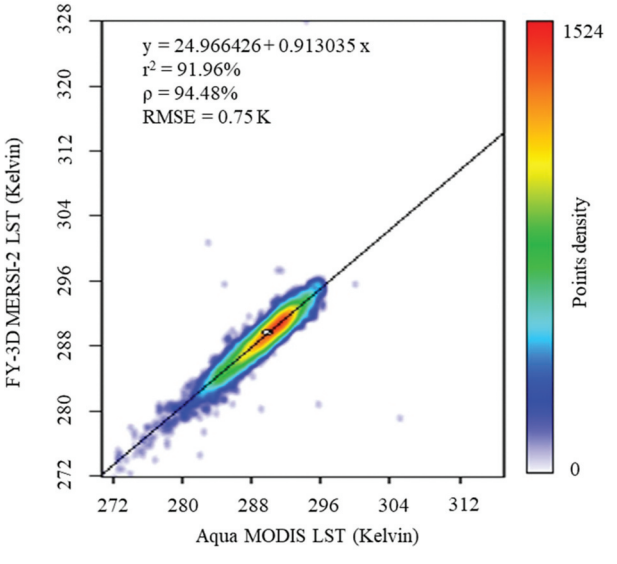

Figure 5. Density plot showing the relationship between MODIS and MERSI-2 LST values over 29,869 data points (from Figure 4). Each data point relates to corresponding pixels as imaged by each sensor.

extracted LST data from Figure 4 and 5 (see Figure 6) reveal that the main source of discrepancy is a higher frequency of slightly higher temperature pixels being isolated by MODIS, while the overall peak LST, as detected by MERSI-2, is higher. The strength of agreement, however, does appear to be spatially variant, with Figure 7 showing pixel-level discrepancies and revealing that these are highest in areas of steep topography – most particularly on the flanks of Mount Etna. This is confirmed in Figure 8 and 9 which plot LST transects over the mountain and showing marked discrepancies on the volcano's steeply rising flanks. Figure 8 also shows the LST retrievals of both sensors compared with their maximum temperature detection limit (i.e. saturation temperature). Reassuringly

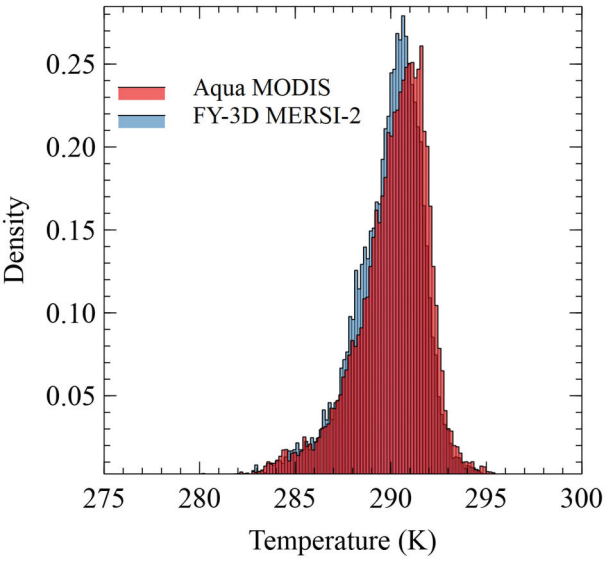

Figure 6. Statistical distribution of LST from the data in Figure 4. Mean temperatures are 290.0 K and 289.8 K for MODIS and MERSI-2, respectively.

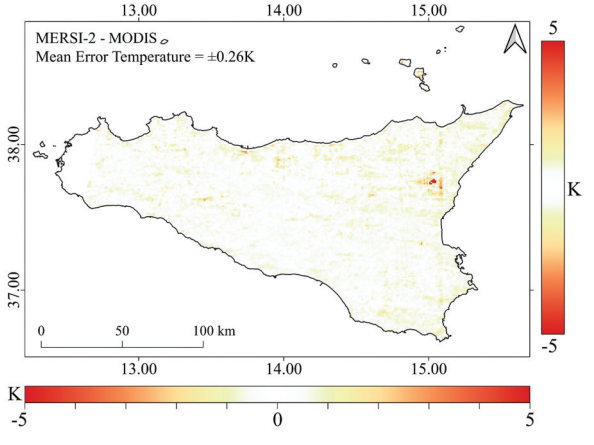

Figure 7. Temperature discrepancy (in Kelvin) between MODIS (Aqua) and MERSI-2. the μT for the whole scene is 0.26 K.

from the perspective of quantitative analysis, even when imaging these active volcanic processes, saturation was never reached for either sensor, with the highest temperature detected by MODIS being 317.28 K as compared with the highest MERSI-2 temperature of 328.09 K (Figure 8).

To understand the influence of topography on the discrepancies between MODIS and MERSI-2 LST retrievals, it is important to understand that pixel-level temperatures are derived from the average of surface temperatures within each pixel's 1 km × 1 km field of view. On viewing topographically steep surfaces, even slightly offset pixels will view surfaces of different altitude and temperature, hence rendering such discrepancies as

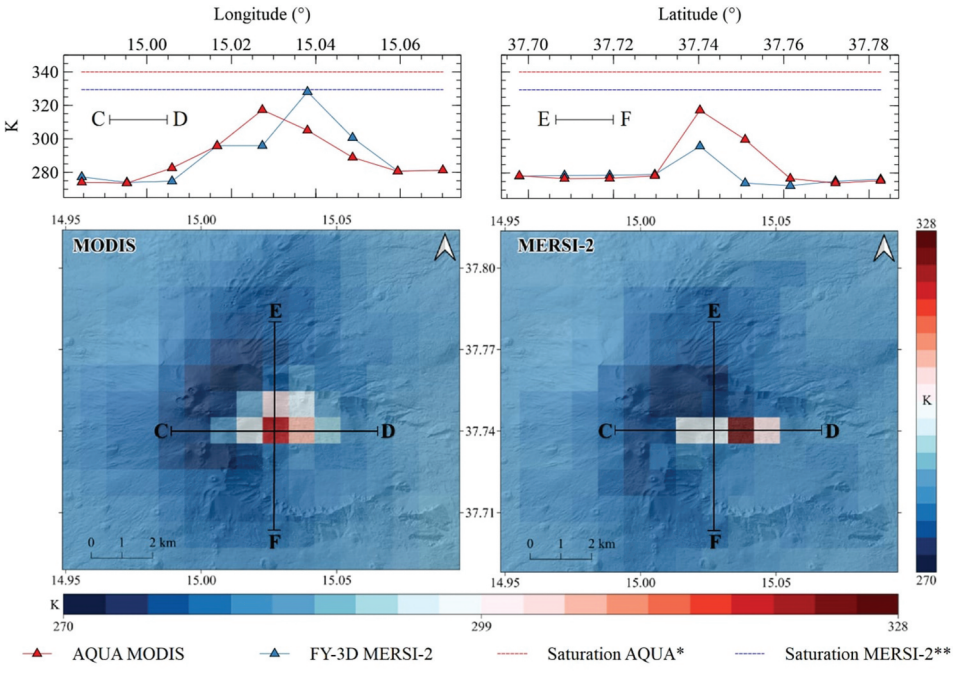

Figure 8. (Top) Temperature differences along a vertical and horizontal transects over Etna crossing the active lava flow. (Bottom) Temperatures (in K) retrieved from MODIS and MERSI-2. Levels of saturation are also displayed for each sensor: 340 K for MODIS Aqua (Pinheiro et al. 2007*) and 329.4 for MERSI-2 (empirically derived from Wang et al. 2019a**).

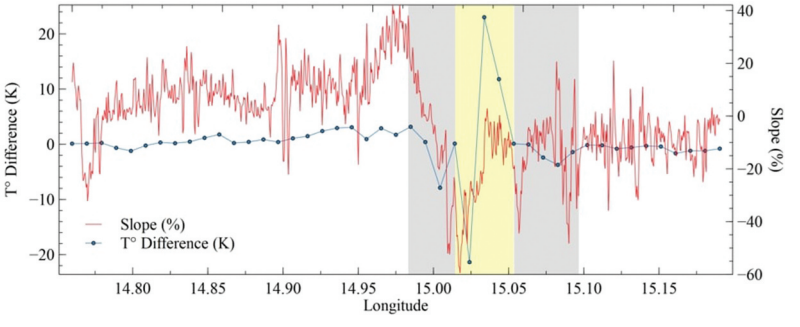

Figure 9. Discrepancies in LST between MODIS and MERSI-2, over Etna, as associated with the slope of the ground. Grey shaded areas represent the beginning of the volcanic edifice (note the change in slope); the yellow shaded area highlights the lava flow.

much more common. The discrepancy evident at the summit of the volcano therefore (i.e. Figure 7), will be partly attributable to these phenomena. The influence of the 20-min gap between image acquisitions must also be considered, with Venzke (2019) showing that Etna was in a particularly active state during this period, displaying Strombolian activity and lava effusion. Such active lava flows at Mount Etna have been shown to have thermal emission variability on the scale of minutes (Bailey et al. 2006). This means that only

complete temporal coincidence of remotely sensed volcanic imagery could result in complete agreement, thus offering an additional explanation for the largest LST discrepancies as seen at the active peak of Mount Etna during this time.

4. Discussion

This initial LST comparison for all of Sicily suggests that MERSI-2 and MODIS TIR data are quasi-equivalent in terms of their capacity for thermal remote sensing of Earth surfaces at ambient temperatures and this is in-spite of some of the assumptions made in the methods applied. Having established this equivalence, the applicability of the MERSI-2 sensor for TIR volcanic observations has also been confirmed, with a positive comparison to corresponding MODIS imagery of Mount Etna having been established. It has been shown that, despite visualizing an active lava flow, neither the pixels of MERSI-2 nor MODIS were saturated, which is encouraging for the volcanological remote sensing community. Considering the range of bands available at 1 km resolution, and those at 250 m resolution (including TIRs at 10.8 and 12.0 μm), MERSI-2 might be particularly useful in monitoring thermal volcanic activity by providing higher-resolution images in TIR channels (as compared with MODIS) while at the same time, also increasing the availability of unsaturated satellite data to monitor the evolution of volcanic events.

We were fortunate in the data presented here that the gap between MODIS and MERSI-2 observations was only 20 min but even in this time, discrepancies in temperature detections were observed. These discrepancies are partly explainable by a variation in lava effusion rates. For example, Harris et al. (2009) showed that a decrease in the lava effusive rates results in the development of a cooler, hardened outer layer. This outer layer traps the heat while also allowing the liquid lava flow freely, thereby reducing the emissions of heat and resulting in a cooler surface temperature detections (Gray Burton-Johnson and Fretwell 2019; Ramsey et al. 2019). Such changes can readily happen on the scale of tens of minutes (Blackett 2014). Despite this, this evidence of relatively comparable observations, even when acquisitions are separated by tens of minutes, might be of significance when included, for instance, in already operating remote volcanic-observation systems, such as HOTSAT (Ganci, Vicari and Negro 2011) or MIROVA (Coppola et al. 2015) and/or those utilizing satellite-derived Time Averaged Discharge Rates (TADR) (Bonny et al. 2018).

5. Conclusion

In this preliminary study we have examined the capacity of MERSI-2's FY-3D instrument for observing and quantifying active volcanic surfaces using its TIR bands, based on imagery of a 2019 eruption at Mount Etna. After converting the MERSI-2 data to LST, we compared it with a near-concurrent scene obtained from the MODIS Aqua sensor. Similarity of the LSTs derived for the whole of Sicily was confirmed, finding $r^2 = 91.96\%$, $\Delta T = 0.26$ K and RMSE = 0.75. Endorsement of MERSI-2 data for quantitative observations of volcanic activity, is also confirmed, as compared with MODIS data retrievals. Discrepancies in the temperature maxima of each scene (317.28 K and 328.09 K for MODIS and MERSI-2, respectively) were found, however. It is suggested that such discrepancies were the result of variations in lava effusion rates, therefore highlighting the

importance of TIR volcanic monitoring, and the importance of new spaceborne platforms for reducing the temporal gaps between image acquisitions. Indeed, there is every possibility that the MERSI-2 data could be integrated into already-operative volcanic monitoring systems or employed to elaborate the retrieval of TADRs, thereby allowing for better volcano monitoring. Such developments will allow scientists and researchers to better understand the dynamics, eruptive regimes and risks posed by volcanoes worldwide.

Within this paper, we also provided a guidance for processing FY-3D MERSI-2 imagery, given that official guidance could not be found. We hope this will facilitate and encourage the use of FY-3D data in future research. Future studies should further investigate the applicability of MERSI-2 for monitoring volcanic activity, considering the benefits of its usage and the contribution that it can make to the field of volcanic remote sensing.

Disclosure statement

No potential conflict of interest was reported by the author(s).

ORCID

S. Aveni http://orcid.org/0000-0003-0661-6749
M. Blackett http://orcid.org/0000-0002-8670-1558

References

Abdelmalik, K. W. 2018. "Role of Statistical Remote Sensing for Inland Water Quality Parameters Prediction." *The Egyptian Journal of Remote Sensing and Space Science* 21 (2): 193–200. doi:10.1016/j.ejrs.2016.12.002.

Anul Haq, M., K. Jain, and K. P. R. Menon. 2012. "Surface Temperature Estimation of Gangotri Glacier Using Thermal Remote Sensing." *International Archives of the Photogrammetry, Remote Sensing and Spatial Information Sciences* 39: 115–119. doi:10.5194/isprsarchives-XXXIX-B8-115-2012.

Bailey, J. E., A. J. L. Harris, J. Dehn, S. Calvari, and S. K. Rowland. 2006. "The Changing Morphology of an Open Lava Channel on Mt. Etna." *Bulletin of Volcanology* 68 (6): 497–515. doi:10.1007/s00445-005-0025-6.

Blackett, M. 2014. "Early Analysis of Landsat-8 Thermal Infrared Sensor Imagery of Volcanic Activity." *Remote Sensing* 6: 2282–2295. doi:10.3390/rs6032282.

Blackett, M. 2015. "An Initial Comparison of the Thermal Anomaly Detection Products of MODIS and VIIRS in Their Observation of Indonesian Volcanic Activity." *Remote Sensing of Environment* 171: 75–82. doi:10.1016/j.rse.2015.10.002.

Blackett, M. 2017. "An Overview of Infrared Remote Sensing of Volcanic Activity." *Journal Of Imaging* 3 (2): 13. doi:10.3390/jimaging3020013.

Blackett, M. and M. J. Wooster. 2011. "Evaluation of SWIR-Based Methods for Quantifying Active Volcano Radiant Emissions Using NASA EOS-ASTER Data." *Geomatics, Natural Hazards and Risk* 2: 51–78. doi:10.1080/19475705.2010.541501.

Bonny, E., T. Thordarson, R. Wright, A. Höskuldsson, and I. Jónsdóttir. 2018. "The Volume of Lava Erupted During the 2014 to 2015 Eruption at Holuhraun, Iceland: A Comparison Between Satellite- and Ground-based Measurements." *Journal of Geophysical Research: Solid Earth* 123 (7): 5412–5426. doi:10.1029/2017JB015008.

Bustamante J, Aragonés D, Afán I, Luque CJ, Pérez-Vázquez A, Castellanos EM, Díaz-Delgado R. 2016. "Hyperspectral Sensors as a Management Tool to Prevent the Invasion of the Exotic Cordgrass Spartina densiflora in the Doñana Wetlands." *Remote Sensing* 8(12): 1001. doi:10.3390/rs8121001.

Carr, B. B., A. Clarke, and L. Vanderkluysen. 2016. "The 2006 Lava Dome Eruption of Merapi Volcano (Indonesia): Detailed Analysis Using MODIS TIR." *Journal of Volcanology and Geothermal Research* 311: 60–71. doi:10.1016/j.jvolgeores.2015.12.004.

CGMS (Coordination Group for Meteorological Satellites). 2018. "Updated Report on Fengyun Satellite Program and Development." CGMS-46 CMA-WP-01. Prepared by CMA, May, 2018, Agenda Item D.

CGMS (Coordination Group for Meteorological Satellites). 2020. "CMA Status of Implementation of CGMS Best Practices in Support to Local and Regional Processing of LEO Direct Broadcast Data." CGMS-48-CMA-WP-04. Prepared by NSMC/CMA.

Coppola, D., M. Laiolo, C. Cigolini, D. Delle Donne, and M. Ripepe. 2015. "Enhanced Volcanic Hot-Spot Detection Using MODIS IR Data: Results from the MIROVA System." *Geological Society, London, Special Publications* 426: 181–205. doi:10.1144/SP426.5.

Coppola, D., D. Piscopo, M. Laiolo, C. Cigolini, D. Delle Donne, and M. Ripepe. 2012. "Radiative Heat Power at Stromboli Volcano During 2000–2011: Twelve Years of MODIS Observations." *Journal of Volcanology and Geothermal Research* 215: 48–60. doi:10.1016/j.jvolgeores.2011.12.001.

Corradino, C., G. Ganci, G. Bilotta, A. Cappello, C. Del Negro, and L. Fortuna. 2019. "Infrared Remote Sensing of Volcanic Activity Using Sentinel-3 Images." *Geophysical Research Abstracts* 21: EGU2019-1226–1.

Dar, I., J. Qadir, and A. Shukla. 2019. "Estimation of LST from Multisensor Thermal Remote Sensing Data and Evaluating the Influence of Sensor Characteristics." *Annals of GIS* 25 (3): 263–281. doi:10.1080/19475683.2019.1623318.

DiStasio, R. J., Jr. and R. G. Resmini. 2010. "Atmospheric Compensation of Thermal Infrared Hyperspectral Imagery with the Emissive Empirical Line Method and the In-Scene Atmospheric Compensation Algorithms: A Comparison." Proc. SPIE 7695, Algorithms and Technologies for Multispectral, Hyperspectral, and Ultraspectral Imagery XVI, 76952B (12 May 2010). doi: 10.1117/12.849898.

Dong, C., J. Yang, W. Zhang, Z. Yang, N. Lu, J. Shi, P. Zhang, Y. Liu, and B. Cai. 2009. "An Overview of a New Chinese Weather Satellite FY-3A." *Bulletin of the American Meteorological Society* 90 (10): 1531–1544. doi:10.1175/2009BAMS2798.1.

ENVI-IDL Technology Hall. 2014. "Geometric Correction of Fengyun-3 Satellite Image Based on GLT Method Under ENVI5.1". Accessed 15 September 2021. http://blog.sina.com.cn/s/blog_764b1e9d0101da96.html.

EOportal. 2021. "FY-3 Eoportal Directory (Official Website)." Accessed 15 September 2021. https://directory.eoportal.org/web/eoportal/satellite-missions/f/fy-3.

Fang, X. 2018. "The Current Status of FY-3D." *Proceedings of Fourth Session of the Inter-Programme Expert Team on Satellite Utilization and Products (IPET-SUP-4/Doc. 5.4)*. WMO HQ, Geneva, 26 February - 1 March 2018.

Francis, P. W. and D. A. Rothery. 1987. "Using the Landsat Thematic Mapper to Detect and Monitor Active Volcanoes: An Example from Lascar Volcano, Northern Chile." *Geology* 15 (7): 614–617. doi:10.1130/0091-7613(1987)15<614:UTLTMT>2.0.CO;2.

Ganci, G., A. Vicari, and C. Negro. 2011. "The HOTSAT Volcano Monitoring System Based on a Combined Use of SEVIRI and MODIS Multispectral Data." *Annals of Geophysics* 54. doi:10.4401/ag-5338.

Gray, D. M., A. Burton-Johnson, and P. T. Fretwell. 2019. "Evidence for a Lava Lake on Mt. Michael Volcano, Saunders Island (South Sandwich Islands) from Landsat, Sentinel-2 and ASTER Satellite Imagery." *Journal of Volcanology and Geothermal Research* 379: 60–71. doi:10.1016/j.jvolgeores.2019.05.002.

Gupta, R. P. 2003. *Remote Sensing Geology*. 2nd ed. GermanyBerlin: Springer-Verlag. doi:10.1007/978-3-662-05283-9.

GVP. 2019.*Global Volcanism Program*. Etna in Volcanoes of the World, v. 4.10.2. edited by E. Venzke. Smithsonian Institution. doi:10.5479/si.GVP.VOTW4-2013.

Harris, A. J. L. and S. K. Rowland. 2009. "Effusion Rate Controls on Lava Flow Length and the Role of Heat Loss: A Review." In *Studies in Volcanology: The Legacy of George Walker* () , edited by T. Thordarson, S. Self, G.Larsen, S. K. Rowland. Special Publications of IAVCEI, vol. 2, pp. 33– 51. Geological Society, London.

Hirn, B., C. Di Bartola, G. Laneve, E. Cadau, and F. Ferrucci. 2008. "SEVIRI Onboard Meteosat Second Generation, and the Quantitative Monitoring of Effusive Volcanoes in Europe and Africa." *Proceedings of 2008 IEEE International Geoscience and Remote Sensing Symposium (IGARSS)*, Boston, MA, USA, pp. 374–377.

Johnson, B. R. and S. J. Young 1998. *In-Scene Atmospheric Compensation: Application to SEBASS Data Collected at the ARM Site*. Technical Report, Space and Environment Technology Center, The Aerospace Corporation.

Kim, J.-I., M.-J. Jun, C.-H. Yeo, K.-H. Kwon, and J. Y. Hyun. 2019. "The Effects of Land Use Zoning and Densification on Changes in Land Surface Temperature in Seoul." *Sustainability* 11 (24): 7056. doi:10.3390/su11247056.

Lu, Q., J. Hu, C. Wu, C. Qi, S. Wu, N. Xu, L. Sun, et al. 2020. "Monitoring the Performance of the Fengyun Satellite Instruments Using Radiative Transfer Models and NWP Fields". *Journal of Quantitative Spectroscopy & Radiative Transfer* 255: 107239. 10.1016/j.jqsrt.2020.107239.

Mao, K. B., Z. Qin, J. Shi, and P. Gong. 2005. "A Practical Split-Window Algorithm for Retrieving Land Surface Temperature from MODIS Data." *International Journal of Remote Senssing* 26: 3181–3204. doi:10.1080/01431160500044713.

Marchese, F., M. Neri, A. Falconieri, T. Lacava, G. Mazzeo, N. Pergola, and V. Tramutoli. 2018. "The Contribution of Multi-Sensor Infrared Satellite Observations to Monitor Mt. Etna (Italy) Activity During May to August 2016." *Remote Sensing* 10 (12): 1948. doi:10.3390/rs10121948.

Massimetti, F., D. Coppola, M. Laiolo, S. Valade, C. Cigolini, and M. Ripepe. 2020. "Volcanic Hot-Spot Detection Using SENTINEL-2: A Comparison with MODIS–MIROVA Thermal Data Series." *Remote Sensing* 12 (5): 820. doi:10.3390/rs12050820.

MCST. 2017. *MODIS 1km Calibrated Radiances Product. NASA MODIS Adaptive Processing System*. USA: Goddard Space Flight Center. doi:10.5067/MODIS/MYD021KM.061.

Meng, Z., Y. Sun, and Y. Dong. 2002. "FY-3 China's Second Generation Polar Orbit Meteorological Satellite." Proceedings of 53rd IAC and World Space Congress, Oct. 10-19, 2002, Houston, TX, IAC-02-B.2.10.

Mincapilli, M., S. Consoli, D. Vanella, G. Ciraolo, and A. Motisi. 2016. "A Time Domain Triangle Method Approach to Estimate Actual Evapotranspiration: Application in a Mediterranean Region Using MODIS and MSG-SEVIRI Products." *Remote Sensing of Environment* 174: 10–23. doi:10.1016/j.rse.2015.12.018.

Murphy, S. W., R. Wright, C. Oppenheimer, and C. R. Souza Filho. 2013. "MODIS and ASTER Synergy for Characterizing Thermal Volcanic Activity." *Remote Sensing of Environment* 131: 195–205. doi:10.1016/j.rse.2012.12.005.

Na, X. 2018. "FY-3D MERSI-II Channel Spectral Response Function and Channel Center Wavelength Usage Guide". (Version 2.0, 2018.07) (in Chinese). Accessed 15 September 2021. http://gsics.nsmc.org.cn/download/documents/SRF/FY3D_MERSI_SRF_V2_201807.pdf.

Na, X. 2019. "Fengyun-3 (Batch 02) Meteorological Satellite Ground Application System Project D Star Medium Resolution Spectral Imager - FY3 Data Product Feature Card." L1 Data Product. Data Usage Guidelines (Version 2.1, 2019.07) (In Chinese).

Na, X., N. Xinhua, H. Xiuqing, W. Xianghua, W. Ronghua, C. Shuaishuai, C. Lin, S. Ling, et al. 2018. "*Prelaunch Calibration and Radiometric Performance of the Advanced MERSI II on FengYun-3D*." IEEE Transactions on Geoscience and Remote Sensing. 1–10. doi:10.1109/TGRS.2018.2841827.

Nádudvari, Á., A. Abramowicz, R. Maniscalco, and M. Viccaro. 2020. "The Estimation of Lava Flow Temperatures Using Landsat Night-Time Images: Case Studies from Eruptions of Mt. Etna and Stromboli (Sicily, Italy), Kīlauea (Hawaii Island), and Eyjafjallajökull and Holuhraun (Iceland)." *Remote Sensing* 12 (16): 2537. doi:10.3390/rs12162537.

NASA LP DAAC. 2015. *MYD11A1 Modis/aqua Land Surface Temperature and the Emissivity Daily L3 Global 1km SIN Grid*. NASA LP DAAC. doi:10.5067/MODIS/MYD11A1.006.

Neri, M., M. De Maio, S. Crepaldi, E. Suozzi, M. Lavy, F. Marchionatti, S. Calvari, and M. F. Buongiorno. 2017. "Topographic Maps of Mount Etna's Summit Craters, Updated to December 2015." *Journal of Maps* 13 (2): 674–683. doi:10.1080/17445647.2017.1352041.

NSMC. 2013. "Chinese National Satellite Meteorological Centre's Fengyun Satellite Data Center." Last accessed 15 September 2021. https://satellite.nsmc.org.cn/portalsite/default.aspx.

NSMC. 2018. "FY-3D Satellite' National Satellite Meteorological Center". Last accessed 15 September 2021. https://fy4.nsmc.org.cn/nsmc/en/satellite/FY3D.html.

Oppenheimer, C. 1998. "Review Article: Volcanological Applications of Meteorological Satellites." *International Journal of Remote Sensing* 19 (15): 2829–2864. doi:10.1080/014311698214307.

Pieri, D. and M. Abrams. 2005. "ASTER Observations of Thermal Anomalies Preceding the April 2003 Eruption of Chikurachki Volcano, Kurile Islands, Russia." *Remote Sensing of Environment* 99: 84–94. doi:10.1016/j.rse.2005.06.012.

Pinheiro, A. C. T., J. Descloitres, J. L. Privette, J. Susskind, L. Iredell, and J. Schmaltz. 2007. "Near-Real Time Retrievals of Land Surface Temperature Within the MODIS Rapid Response System." *Remote Sensing of Environment* 106: 326–336. doi:10.1016/j.rse.2006.09.006.

Ramsey, M., M. Chevrel, D. Coppola, and A. Harris. 2019. "The Influence of Emissivity on the Thermo-Rheological Modeling of the Channelized Lava Flows at Tolbachik Volcano." *Annals of Geophysics*. doi:10.4401/ag-8077.

Rogic, N., A. Cappello, and F. Ferrucci. 2019. "Role of Emissivity in Lava Flow 'Distance-To-Run' Estimates from Satellite-Based Volcano Monitoring." *Remote Sens* 11 (6): 662. doi:10.3390/rs11060662.

Rothery, D. A., D. Coppola, and C. Saunders. 2005. "Analysis of Volcanic Activity Patterns Using MODIS Thermal Alerts." *Bulletin of Volcanology* 67: 539–556. doi:10.1007/s00445-004-0393-3.

Rothery, D. A., P. W. Francis, and C. A. Wood. 1988. "Volcano Monitoring Using Short Wavelength Infrared Data from Satellites." *Journal of Geophysical Research* 93 (B7): 7993–8008. doi:10.1029/JB093iB07p07993.

Singh, V., R. Satpathy, and A. Jeyaseelan. 2010. "Spatial Variation of Vegetation Moisture Mapping Using Advanced Spaceborne Thermal Emission & Reflection Radiometer (ASTER) Data." *Journal of Environmental Protection* 1: 448–455. doi:10.4236/jep.2010.14052.

Trifonov, G. M., M. N. Zhizhin, D. V. Melnikov, and A. A. Poyda. 2017. "VIIRS Nightfire Remote Sensing Volcanoes." *Procedia Computer Science* 119: 307–314. doi:10.1016/j.procs.2017.11.189.

Vieira, D., A. Teodoro, and A. Gomes 2016. "Analyzing Land Surface Temperature Variations During Fogo Island (Cape Verde) 2014-2015 Eruption with Landsat 8 Images". *Proceedings Volume 10005, Earth Resources and Environmental Remote Sensing/GIS Applications VII*; 1000508. doi: 10.1117/12.2241382.

Wan, Z. and W. Snyder. 1996. "MODIS Land-Surface Temperature Algorithm Theoretical Basis Document". (LST ATBD), Version 3.2."

Wang, M., G. He, Z. Zhang, G. Wang, Z. Wang, R. Yin, S. Cui, et al. 2019b. "A Radiance-Based Split-Window Algorithm for Land Surface Temperature Retrieval: Theory and Application to MODIS Data". *International Journal of Applied Earth Observation and Geoinformation* 76: 204–217. 10.1016/j.jag.2018.11.015.

Wang, L., X. Hu, N. Xu, and L. Chen. 2020. "Water Vapor Retrievals from Near-Infrared Channels of the Advanced Medium Resolution Spectral Imager Instrument Onboard the Fengyun-3D Satellite." *Advances in Atmospheric Science* 38: 1351–1366. doi:10.1007/s00376-020-0174-8.

Wang, H., K. Mao, F. Mu, J. Shi, J. Yang, Z. Li, and Z. Qin. 2019a. "A Split Window Algorithm for Retrieving Land Surface Temperature from FY-3D MERSI-2 Data." *Remote Sensing* 11: 2083. doi:10.3390/rs11182083.

Wang, D., Y. Tian, S. Qiang, Q. Du, X. Wang, W. Bai, X. Meng, et al. 2018. "Preliminary In-Orbit Evaluation of Gnos on FY3D Satellite." IGARSS 2018 - 2018 IEEE International Geoscience and Remote Sensing Symposium, 2018, 9161–9163. doi:10.1109/IGARSS.2018.8518927.

Watson, I. M., V. J. Realmuto, W. I. Rose, A. J. Prata, G. J. S. Bluth, Y. Gu, C. E. Bader, and T. Yu. 2004. "Thermal Infrared Remote Sensing of Volcanic Emissions Using the Moderate Resolution Imaging Spectroradiometer." *Journal of Volcanology and Geothermal Research* 135: 75–89. doi:10.1016/j.jvolgeores.2003.12.017.

Wien, W. 1896. "Uber Die Energieverteilung in Emissionspektrum Eines Schwarzen Korpers." *Annals of Physics* 58: 662–669.

Wooster, M. and D. Rothery. 1997. "Thermal Monitoring of Lascar Volcano, Chile, Using Infrared Data from the Along-Track Scanning Radiometer: A 1992-1995 Time Series." *Bulletin of Volcanology* 58: 566–579. doi:10.1007/s004450050163.

Wright, R., L. Flynn, H. Garbeil, A. Harris, and E. Pilger. 2002. "Automated Volcanic Eruption Detection Using MODIS." *Remote Sensing of Environment* 82 (1): 135–155. doi:10.1016/S0034-4257(02)00030-5.

Wright, R., L. Flynn, H. Garbeil, A. J. L. Harris, and E. Pilger. 2004. "MODVOLC: Near-Real-Time Thermal Monitoring of Global Volcanism." *Journal of Volcanology and Geothermal Research* 135 (1–2): 29–49. doi:10.1016/j.jvolgeores.2003.12.008.

Wright, R., L. P. Flynn, and A. J. Harris. 2001. "Evolution of Lava Flow-Fields at Mount Etna, 27–28 October 1999, Observed by Landsat 7 ETM+." *Bulletin of Volcanology* 63: 1–7. doi:10.1007/s004450100124.

Wright, R., L. Glaze, and S. M. Baloga. 2011. "Constraints on Determining the Eruption Style and Composition of Terrestrial Lavas from Space." *Geology* 39: 1127–1130. doi:10.1130/G32341.1.

Yan, L., Y. Hu, Y. Zhang, X.-M. Li, C. Dou, J. Li, Y. Si, and L. Zhang. 2021. "Radiometric Calibration Evaluation for FY3D MERSI-II Thermal Infrared Channels at Lake Qinghai." *Remote Sensing* 13 (3): 466. doi:10.3390/rs13030466.

Yang, J., L. Jiang, S. Wu, G. Wang, J. Wang, and X. Liu. 2019a. "Development of a Snow Depth Estimation Algorithm Over China for the FY-3D/MWRI." *Remote Sensing* 11: 977. doi:10.3390/rs11080977.

Yang, Z., P. Zhang, S. Gu, X. Hu, S. Tang, L. Yang, N. Xu, et al. 2019b. "Capability of Fengyun-3D Satellite in Earth System Observation". *Journal of Meteorological Research* 33: 1113–1130. 10.1007/s13351-019-9063-4.

Young, S. J., B. R. Johnson, and J. A. Hackwell. 2002. "An In-Scene Method for Atmospheric Compensation of Thermal Hyperspectral Data." *Journal of Geophysical Research* 107 (D24): 4774. doi:10.1029/2001JD001266.

Zhang, P. 2019. "Fengyun Meteorological Satellites and Consideration on Calibration Issues." 99th AMS Annual Meeting 8 Jan., 2019, Phoenix, USA.

Zhang, Y.-X., X. Li, M. Zhang, Q. Kang, W. Wei, X.-B. Zheng, and Y. Zhang. 2020. "On-Orbit Radiometric Calibration for Thermal Infrared Band of FY3D/MERSI-II Satellite Remote Sensor Based on Qinghai Lake Radiation Calibration Test-Site." *Acta Photonica Sinica* 49(5): 528002-0528002 in Chinese. doi:10.3788/gzxb20204905.0528002.